Cellulose (2020) 27:7677–7689
https://doi.org/10.1007/s10570-020-03311-6

ORIGINAL RESEARCH

Methylcellulose strengthened polyimide aerogels with excellent oil/water separation performance

Longhai Zhuo · Cong Ma · Fan Xie · Shanshan Chen · Zhaoqing Lu

Received: 22 April 2020 / Accepted: 24 June 2020 / Published online: 1 July 2020

Abstract Polyimide (PI) aerogels have great potential in oil/water separation field, but the extreme volume shrinkage during the fabrication still remains challenging. Herein, a simple yet efficient strategy of incorporating methylcellulose (MC) in PI aerogels is proposed. The MC/PI composite aerogels were fabricated by freeze-drying plus thermal imidization with subsequent trimethylchlorosilane (TMCS) functionalization. The results revealed that MC entered the skeleton of aerogels and strengthened it effectively by promoting the formation of robust and complete 3D porous structure, and the defects of as-prepared aerogels were eliminated when the proportion of MC was beyond 10 wt%. After modification with TMCS, the water contact angle of aerogels increased significantly by 30°–40°, and the functionalized aerogels showed excellent oil absorption capacity up to 28.44 g/g. The outstanding oil absorbency and simple process for separating oil and water with MC/PI composite aerogels are promising candidates in the field of oil/water separation.

Keywords Polyimide · Methylcellulose · Aerogel · Oil/water separation

Electronic supplementary material The online version of this article (https://doi.org/10.1007/s10570-020-03311-6) contains supplementary material, which is available to authorized users.

L. Zhuo (✉)
Key Laboratory of Auxiliary Chemistry and Technology for Chemical Industry, Ministry of Education, Shaanxi University of Science and Technology, Xi'an 710021, China
e-mail: zhuolonghai@foxmail.com

L. Zhuo
Shaanxi Collaborative Innovation Center of Industrial Auxiliary Chemistry and Technology, Shaanxi University of Science and Technology, Xi'an 710021, China

C. Ma
College of Chemistry and Chemical Engineering, Shaanxi University of Science and Technology, Xi'an 710021, China

F. Xie · S. Chen · Z. Lu
College of Bioresources Chemical and Materials Engineering, Shaanxi University of Science and Technology, Xi'an 710021, China

Introduction

With the rapid development of technology and industry, human beings are confronted with severe environmental pollution (Najafian et al. 2018, 2019; Orooji et al. 2020a, b; Ranjeh et al. 2019, 2020). Particularly, the oil pollution problems caused by petroleum spills and leaks, have attracted the extensive attention of researchers (Gupta et al. 2017; Mehdizadeh et al. 2020; Shahed et al. 2020; Wang et al. 2020a, b). To reduce the environmental and ecological influences, several techniques have been widely used to deal with the oil pollution, such as oil fencing (Hu et al. 2018; Kim et al. 2009), chemical dispersion (Wang et al. 2013; Yan et al. 2019a), superwettable membrane separation (Chu et al. 2015; Lin and Hong 2019; Yan et al. 2019b), bioremediation (Dashti et al. 2019; Ji et al. 2019; Machado et al. 2019), in-situ combustion (Yuan et al. 2019a, b), oil adsorption (Krasian et al. 2019; Parmar et al. 2019; Songsaeng et al. 2019). Among these, the oil adsorption, collected oil spills mainly by physical adsorption, is one of the most ideal and economical ways. To date, extensive research work on oil absorbents has been carried out, and a variety of absorbent materials have been developed, such as activated carbon (Marrakchi et al. 2017), high oil absorbing resin (Sun et al. 2014), bentonites, aerogel materials (Chhajed et al. 2019; El-Shahidy et al. 2019).

Aerogels, a novel class of light porous materials, possess excellent adsorption properties due to the large porosity, which make them promising candidates for oil adsorption (Yang et al. 2019). Beshkar et al. (2020) fabricated a superhydrophobic cotton fabric based on the modified cellulose fibers, which could separate the oily solvent from water with a high separation efficiency beyond 94%. In addition to cellulose (Beshkar et al. 2020; Xu et al. 2019), materials such as graphene (Zhao et al. 2019), methylsilsesquioxane (Guo et al. 2018), polyimide (PI) (Ning et al. 2017), have been successfully applied to the fabrication of oil adsorption aerogels. In recent years, PI has become one of the most attractive organic candidates for aerogels due to the outstanding performance (Chao et al. 2019; Wang et al. 2020c; Zhang et al. 2020). Various efforts have been carried out mainly focusing on the preparation techniques of PI aerogels, such as supercritical CO_2 drying (Shen et al. 2013; Zhai and Jana 2017; Zhang et al. 2016), acetone bath (Kim et al. 2016; Kwon et al. 2014), freeze-drying plus thermal imidization (He et al. 2017). Generally speaking, the freeze-drying plus thermal imidization method, which involves the following three steps: preparation of polyamic acid (PAA) aqueous solution, freeze-drying, and thermal imidization, is more green, simple and convenient, and will facilitate the preparation and potential application of PI aerogels (Chen et al. 2019). However, the aerogels fabricated by this approach usually shrink significantly, thus seriously affecting the performance of the polyimide aerogels, which could be attributed to the weak strength of PAA aerogel skeleton. Accordingly, it is of great significance to improve the skeleton strength of PAA aerogels.

For polymer aerogels, introducing crosslinking structures and reinforcing components are the common ways to enhance the skeleton strength (Ren et al. 2018; Wang et al. 2017; Zhao et al. 2020). However, the amide bond and carboxylic acid of PAA cannot react with anhydrides or amino groups in aqueous solution, and it's difficult to introduce the crosslinking structure simply through ternary anhydrides or amine monomers. Therefore, incorporating the reinforcing components should be more suitable, and the components should have the characteristics of high strength, good compatibility, water dispersion, suitable size and so on (Orooji et al. 2019; Seifi et al. 2020). Methylcellulose (MC), as a kind of cellulose ethers with good water dispersibility, high strength, superfine structure, wide range of sources, is an ideal strengthen filler for aqueous solution system (Boumail et al. 2013; Kumar et al. 2012). The abundant methyl ether and hydroxyl groups of MC could provide good compatibility and strong interfacial interaction with PAA molecular chain (Long et al. 2020; Pinotti et al. 2007). Accordingly, MC could be introduced in the PAA aqueous solution and assembled with the PAA matrix via hydrogen bonding (Bai et al. 2020). Owing to the good compatibility between MC and PAA, MC could be well dispersed in the PAA skeleton and strengthen the aerogel skeleton effectively.

In view of the facts mentioned above, herein MC was introduced into polyimide aerogel as the reinforcing agent, which could provide mechanical support for aerogel skeleton due to its superfine structure and high strength. A series of lightweight and porous methylcellulose/polyimide (MC/PI) aerogels were fabricated by freeze-drying plus thermal imidization

method, and followed by oleophilic modification with trimethylchlorosilane (TMCS), aiming to endow the aerogels with excellent oil absorption capability. The densities, volume shrinkage, microstructures, compression properties and oil absorption capacities of the MC/PI aerogels were studied thoroughly.

Experimental

Materials

3,3′,4,4′-Benzophenonetetracarboxylic dianhydride (BTDA, 99%), MC and TMCS were purchased from Shanghai Macklin Biochemical Co. Ltd (Shanghai, China). 4,4′-Diaminodiphenyl ether (ODA) was obtained commercially from Aladdin Chemistry Co. Ltd. (Shanghai, China). Triethylamine and *N*,*N*-dimethylformamide (DMF) were supplied by Guangdong Guanghua Sci-Tech Co., Ltd (Shantou, China). All the above reagents were used as-received. The deionized water was prepared by Purelab Classic ultra-pure water system.

Preparation of MC aqueous dispersion

MC was dispersed in deionized water by the ultrasonic-assisted heat treatment. Briefly, an appropriate amount of MC was put into 20 mL 70 °C deionized water, and the mixture was treated by ultrasonic for 0.5 h. After treatment, a uniform MC aqueous dispersion was obtained.

Preparation of methylcellulose/polyamic acid aqueous solution

Firstly, ODA (2.00 g, 10 mmol) was dissolved in DMF (25 mL) by magnetic stirring. Then, BTDA (3.22 g, 10 mmol) was added into ODA solution slowly, and the mixture was stirred for 36 h at room temperature. After that, the resulting PAA solution was poured into excess deionized water. The PAA particles were collected by filtration, washed thoroughly with deionized water and ethanol, and followed by freeze-drying. Finally, the PAA particles were dissolved in the MC aqueous dispersion by adding appropriate amount of triethylamine. The concentration of PAA was about 20 mg/mL, and the concentrations of MC were controlled at 0 mg/mL, 1 mg/mL, 2 mg/mL, 3 mg/mL, 4 mg/mL, 5 mg/mL.

Fabrication of MC/PI composite aerogels

The MC/PI composite aerogels were fabricated by freeze-drying together with thermal imidization. Firstly, the MC/PAA aqueous solution was transferred to the mold and frozen by refrigerator. Then, the sample was freeze-dried by the FD-1A-50 freeze dryer after the mixture was completely frozen. Finally, the obtained sample was heated and the MC/PI composite aerogels were obtained through dehydration cyclization. The detailed parameters of thermal imidization were as follows: 120 °C for 0.5 h, 150 °C for 0.5 h, 200 °C for 0.5 h, and 250 °C for 3 h.

Oleophilic modification of the aerogels

The MC/PI composite aerogels were modified by surfactant for hydrophobic and oleophilic performance. Specifically, the aerogels were dipped into the TMCS/ethanol solution for 30 min, and followed by silylation treatment at 70 °C for 2 h. The samples were donated as MC/PIA-1, MC/PIA-2, MC/PIA-3, MC/PIA-4, MC/PIA-5 and MC/PIA-6, respectively. The schematic illustration of the fabrication of MC/PI composite aerogels was shown in Fig. 1.

Characterization

Fourier transform infrared (FT-IR) spectra were recorded on a Bruker Vector-22 fourier transform infrared spectrometer (Germany) with a resolution of 2 cm^{-1} and a scanning range of 500–4000 cm^{-1}. Prior to testing, the samples were pressed to pellets with KBr. Differential scanning calorimetry (DSC) was performed using a TA DSC2-00185 differential scanning calorimeter (America) and recorded from ambient temperature to 350 °C under N_2 atmosphere with a heating rate of 10 °C min^{-1}. Prior to testing, the samples were annealed in the differential scanning calorimeter through the following steps: temperature rise to 250 °C under N_2 atmosphere with a heating rate of 10 °C min^{-1}, heat preservation for 5 min, and then cool to room temperature. Scanning electron microscope (SEM) was carried out with a Hitachi S4800 microscope (Japan). Typically, the samples were measured at 5 kV, with a working distance of 1.9–40

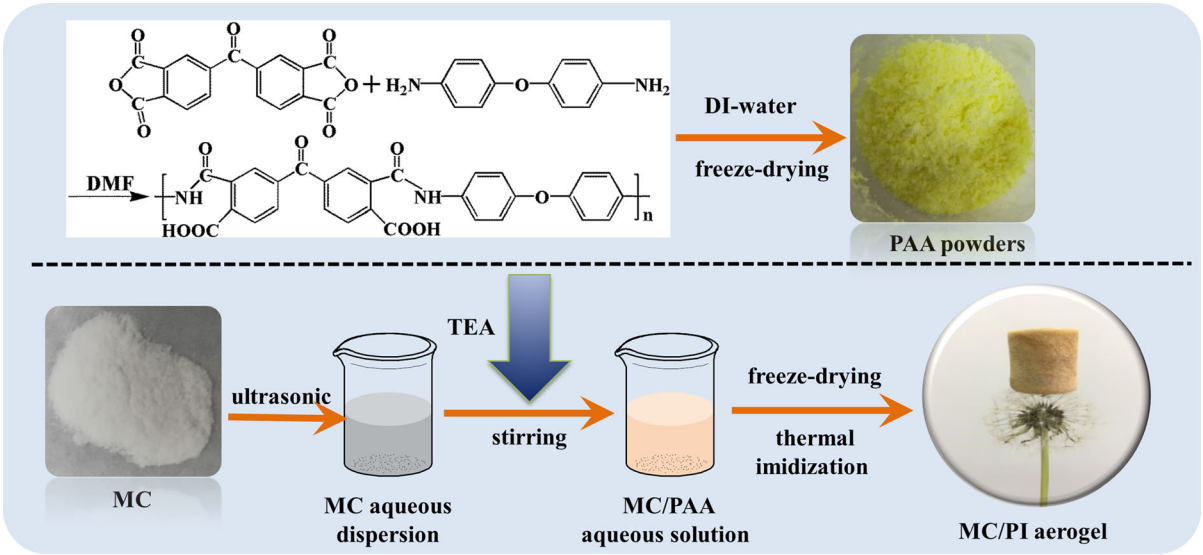

Fig. 1 Schematic illustration of the fabrication of the MC/PI composite aerogels

mm. Prior to imaging, an ultrathin coating of platinum was deposited on the samples by sputtering (sputtering current: 20 mA, sputtering time: 45 s). The compression test was carried on a Baoda Instrument Co., Ltd 1036PC universal testing machine (China) with a compression speed of 2 mm/min. The recovery ratios were obtained by corresponding recovery height of aerogel divided by the initial height. The water contact angle (CA) of the resulting MC/PI composite aerogels was measured on a Kruss DSA100 Contact Angle Measuring Instrument (Germany) at room temperature. The absorption capacities (Q) of the composite aerogels for oil contaminations were estimated by placing a piece of aerogel in the organic liquids for 5 min. The samples were accurately weighted to obtain the initial (M_0) and n^{th} oil absorption mass (M_n). The absorption capacities (Q_n) were calculated as: $Q_n = (-M_n - M_0)/M_0$. The reduced mass of oil after each adsorption was measured, which was recorded as M_{an} for the nth oil absorption process. The discharged oil by extrusion was weighted, and was recorded as M_{dn} for the nth extrusion process. The recovery ratios of the oil for the separation process were calculated as: $R_n = (M_{d1} + M_{d2} + \cdots + M_{dn})/(M_{a1} + M_{a2} + \cdots + M_{an})$.

Results and discussion

The FT-IR spectra of PI aerogel and MC/PI composite aerogels were shown in Fig. 2a). The spectra showed that the characteristic absorption bands of the aromatic imide group appeared around 1780 cm^{-1} ($\gamma_{C=O}$, asymmetrical stretching), 1720 cm^{-1} ($\gamma_{C=O}$, symmetrical stretching), 1365 cm^{-1} (γ_{C-N}, stretching), and 725 cm^{-1} (deformation of imide ring), which demonstrated the formation of imide rings. No obvious characteristic peaks of ammonium carboxylic ester were detected, indicating that the thermal imidization was fully complete. According to the DSC curves (Fig. 2b), MC/PIA-1 and MC/PIA-2 aerogels exhibited a clear endotherm peak around 330 °C, which referred to the glass transition. Meanwhile, no endotherm was found in the DSC curves of the MC/PIA-3, MC/PIA-4, MC/PIA-5 or MC/PIA-6 aerogels. The DSC results manifested the high glass transition temperatures of MC/PIA-1 and MC/PIA-2, and that there was no obvious glass transition for the others.

To further study the effects caused by MC, the densities and volume shrinkage of the composite aerogels were conducted, as shown in Fig. 2c, d. Clearly, the volume shrinkage decreased gradually with increased proportion of MC, indicating the effective reinforcement of MC for aerogel skeleton. In general, the shrinkage of aerogels dwindled obviously, especially for freeze-drying while addition

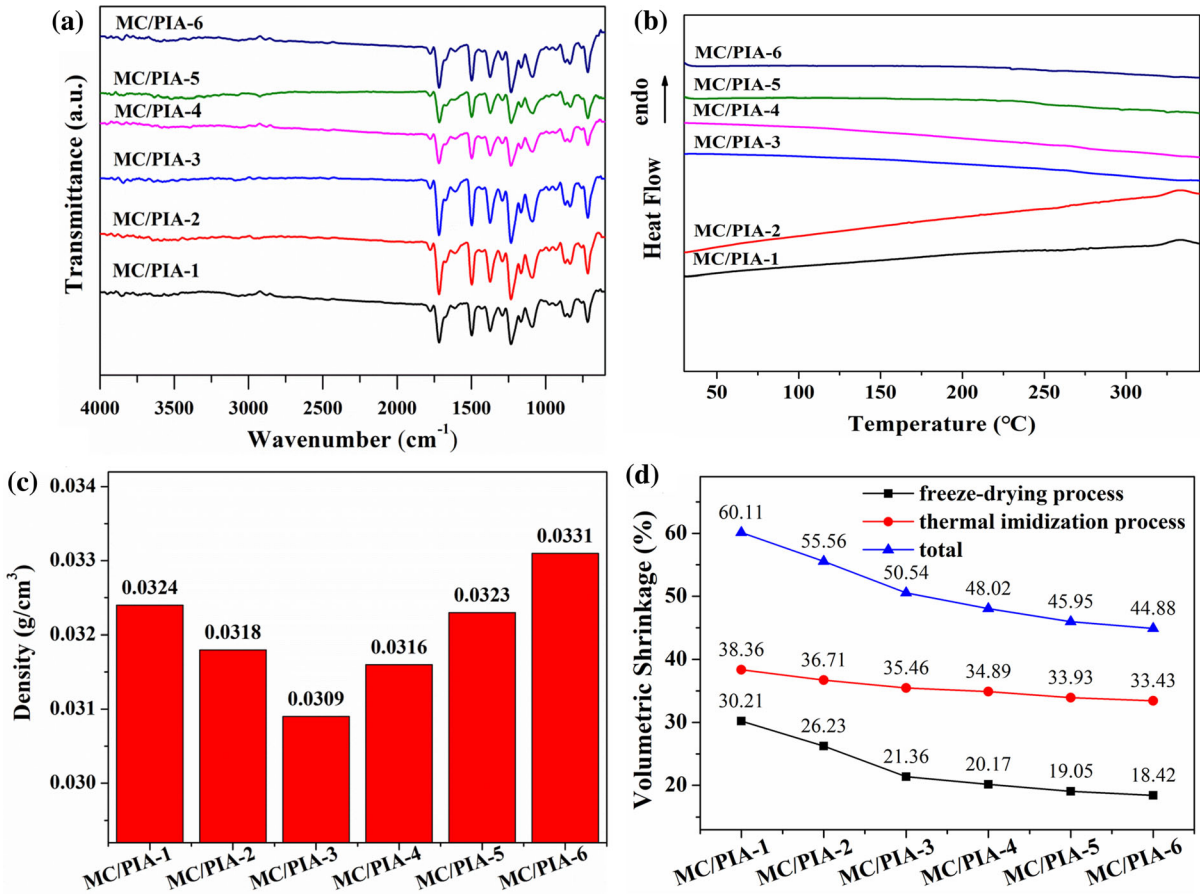

Fig. 2 The FT-IR spectra (**a**), densities (**b**), volumetric shrinkage (**c**) and DSC curves (**d**) of the resulting aerogels

proportion of MC was below 10 wt%. When the addition proportion was beyond 10 wt%, the downward trend of volume shrinkage for freeze-drying processes became relatively slow. For the thermal imidization, the volume shrinkage also decreased with the increase of MC content, but the trend was much slower than that of freeze-drying processes, which might be attributed to the stiffness changes caused by the huge difference in temperature during the two processes. Combine the freeze-drying with thermal imidization, the total volume shrinkage was reduced from 60.11 to 44.88% as the MC proportion increased. Meanwhile, the densities decreased first and then increased, in the range of 0.0309–0.0331 g/cm^3. The densities of the resulting aerogels decreased obviously when the proportion of MC to PAA increased from 0 to 10 wt%, and then increased when the proportions were beyond 10 wt%. The density changes of the as-prepared aerogels could be attributed to the combined effects of mass and volume. Obviously, the introduction of MC could reduce the volume shrinkage of aerogel to get larger volume, but led to an increase in the mass of aerogel. When the proportion of MC was less than 10 wt%, the volume increase played the leading role. When the proportion was beyond 10 wt%, the mass increase dominated.

Figure S1 (Supplementary Material) showed the front, vertical section and across section photographs of MC/PI composite aerogels with different MC content. Overall, the shrinkage of MC/PIA-1 and MC/PIA-2 was much higher than the last four, and the shrinkage of MC/PIA-3 was slightly higher than latter ones, and MC/PIA-4, MC/PIA-5 and MC/PIA-6 composite aerogels were similar and possessed the lowest shrinkage. According to the vertical and across section photographs, some defects were existed in the internal structure of the first two samples and the defects of MC/PIA-1 were much more obvious. For

MC/PIA-3, MC/PIA-4, MC/PIA-5 and MC/PIA-6 composite aerogels, the internal structures were smooth, and there were no apparent defects in the vertical and across section. This phenomenon might be explained by that the skeleton of PAA aerogels was weak, and it was prone to be broken during freeze-drying and thermal imidization. After the incorporation of MC, the aerogel skeleton was strengthened, and the defects gradually disappeared. In other words, the introduction of MC could effectively reduce the volume shrinkage and cure the internal defects of aerogels.

Generally, the introduction of MC could enhance the skeleton strength of PI aerogels, as it could reduce the volume shrinkage and eliminate the internal defects. When the content of MC was 5 wt%, the enhancement effects could effectively reduce the internal defects and volume shrinkage, but it was not enough to completely eliminate the defects. Thus, defects were formed on the skeleton of MC/PIA-1 and MC/PIA-2. When incorporated with 10 wt% MC, the internal defects of aerogels were eliminated, and the decrease of volume shrinkage was much more obvious. When the content of MC was beyond 10 wt%, the enhancement effects were enough to eliminate the apparent defects, and the volume shrinkage of aerogels was stable.

The morphologies of the pure PI aerogel and MC/PI composite aerogels were characterized by SEM, as shown in Fig. 3. It was increasingly clear that the skeleton of MC/PIA-1 and MC/PIA-2 aerogels mainly existed in the form of large longitudinal lamellar, and there were more horizontal connections for MC/PIA-2 than MC/PIA-1. As for MC/PIA-3, MC/PIA-4, MC/PIA-5 and MC/PIA-6, the aerogels exhibited a hierarchically open-cell structure with continuous pores, and the pore size were from 10 to 100 μm. The cell wall was constructed by the interconnected, porous 3D skeleton of randomly oriented MC/PI lamellar structure. In addition, there were no obvious MC rods in the skeleton of the aerogels (see Fig. 4), indicating that MC might be wrapped by PI matrix (or PAA matrix). The results might be attributed to the hydrogen bonding between MC and the PAA molecular chain, thus improving the compatibility between them. MC could enter the skeleton of PAA aerogels and strengthened the lamellar structures effectively, resulting in the decrease of volume shrinkage. In addition, the strengthened skeleton could tend to form thinner lamellar structures and promote the lateral formation of the aerogels. Therefore, the reinforced concrete structure was obtained in the interiors of the as-prepared aerogels, and endowed the aerogels with robust and complete 3D porous structure.

Herein, a series of compression tests were performed to evaluate the reinforcement of MC for the aerogels. The stress-strain curves and recovery ratios shown in Fig. 5 revealed that the compression and recovery properties were significantly enhanced with the increasing MC loading, which further confirmed the validity of MC strengthened PI aerogels. Figure 5c–f demonstrated the stress-strain curves and recovery ratios of the MC/PIA-1 and MC/PIA-3 as a function of compression time. With the increase of compression times, the stress-strain proportion and recovery ratios decreased, but the downward trend gradually slowed down and tended to be stable. Compared with MC/PIA-1, MC/PIA-3 held higher stress-strain proportion and recovery ratios for the same compression time, and possessed lower downward trends. The results might be attributed to the strengthened skeleton and the formation of robust and complete 3D porous structure, which could enhance the compression resistance of the aerogels effectively.

According to the results mentioned above, we interpreted the possible mechanism of MC reinforced PI aerogel. Firstly, MC was wrapped by PAA during the formation of aerogel skeletons. Benefitted from the high strength of MC, the lamellar structure skeletons were strengthened. Meanwhile, MC promoted the lateral formation of the aerogels, and endowed the MC/PAA aerogels with reinforced concrete, 3D porous structure. During freeze-drying, the volume shrinkage decreased significantly due to the strengthened skeletons, and the MC/PAA aerogels with relatively complete 3D porous structure were obtained. As for the thermal imidization, MC softened at high temperature and had weaker enhancement effect on the aerogel skeleton, so volume shrinkage did not decline significantly as the MC content increased. Generally, MC participated in the building of aerogel skeleton and effectively decreased the volume shrinkage of freeze-drying, and promoted the formation of relatively complete 3D porous structures in MC/PI composite aerogels.

To investigate the wettability influence of oleophilic modification, CA measurement was carried out. To minimize the error caused by roughness of surfaces,

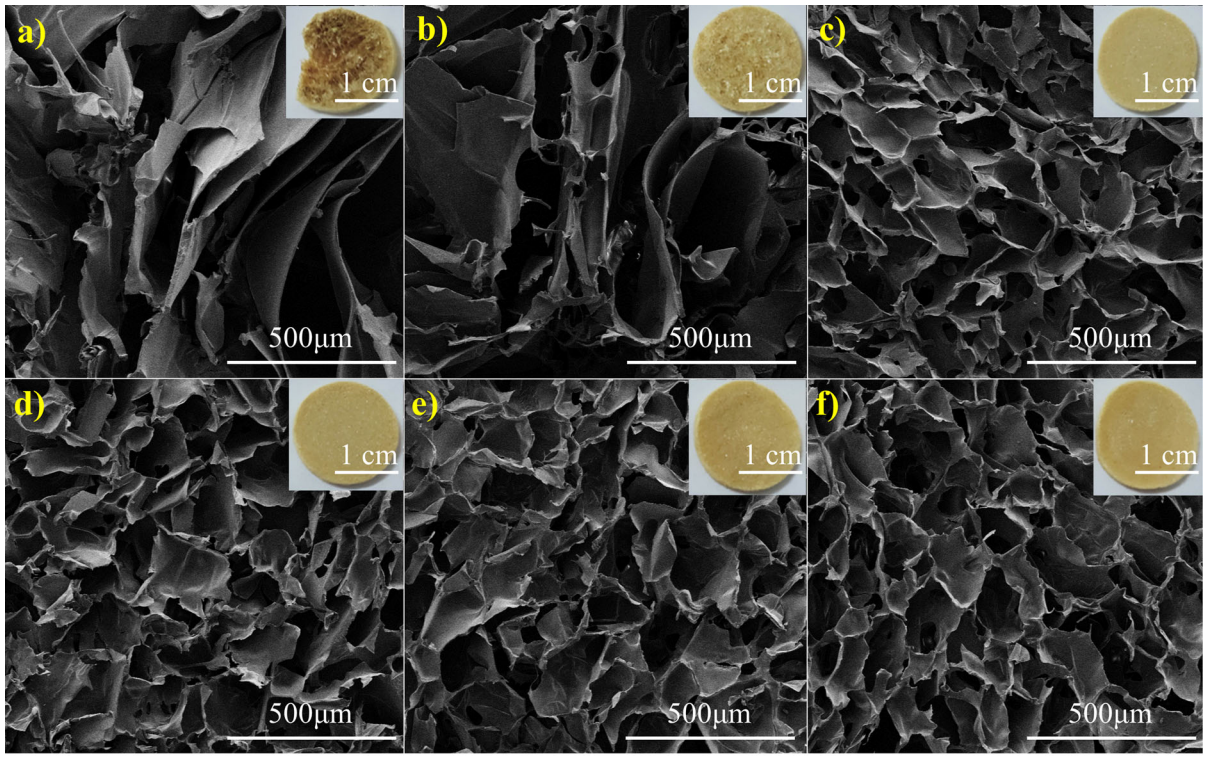

Fig. 3 SEM morphologies of the composite aerogels across sections. **a** MC/PIA-1; **b** MC/PIA-2; **c** MC/PIA-3; **d** MC/PIA-4; **e** MC/PIA-5; **f** MC/PIA-6

CA values were measured 5 times at different points, and the average CA values were shown in Fig. 6a). As a result, the unmodified aerogels held the water CA of about 90°, indicating the weak surface hydrophobicity. After modification, the water CA values of aerogels increased significantly by 30–40°, demonstrating much better surface hydrophobicity than the un-modified ones. The increase of surface hydrophobicity could be regarded as the result of the introduction of oleophilic groups on the surface of aerogel skeleton. Both the unmodified and modified aerogels had the same trend that the water CA value decreased slightly as the content of MC increased due to the better hydrophilicity of MC.

Owing to the low density, high porosity and surface hydrophobicity, the modified MC/PI composite aerogel was considered as a promising oil/water separation material. Figure 6b presented the absorbing oil phenomenon in oil-water system, taking MC/PIA-3 as an example and using methyl silicone oil (dyed with Sudan Red II) as the absorbed oil. Apparently, the oil was completely absorbed by MC/PIA-3 in just about 5 s as MC/PIA-3 contacted with the oil. Figure 7a showed the absorption and discharging processes of the modified MC/PIA-3 aerogel. Once the aerogel was immersed in the silicone oil, the aerogel absorbed the oil and reached saturation rapidly, while sinking to the oil bottom and floating on the water surface. After that, the absorbed oil was discharged by extrusion, and then the aerogels could be used for the next absorption. The oil absorption capacities (Q) were calculated by the measuring method presented in Sect. "Characterization", and the results were listed in the Table S1. For the first absorption, the oil capacities of the as-prepared aerogels were about 25.19–28.44 g/g. The oil capacity was higher than the nanocrystalline cellulose aerogels (16 g/g) (Zhang et al. 2019), and equivalent to the compressible cellulose nanocrystals/PVA aerogels (21.2–32.7 g/g) (Gong et al. 2019), but lower than polyimide/graphene aerogel (34 g/g) (Ren et al. 2019). In addition, according to Figs. 6b and 7a, the as-prepared aerogels could absorb the oil rapidly, and there was no water in the discharged oil, indicating the effectiveness of aerogels for absorbing oil from the oil/

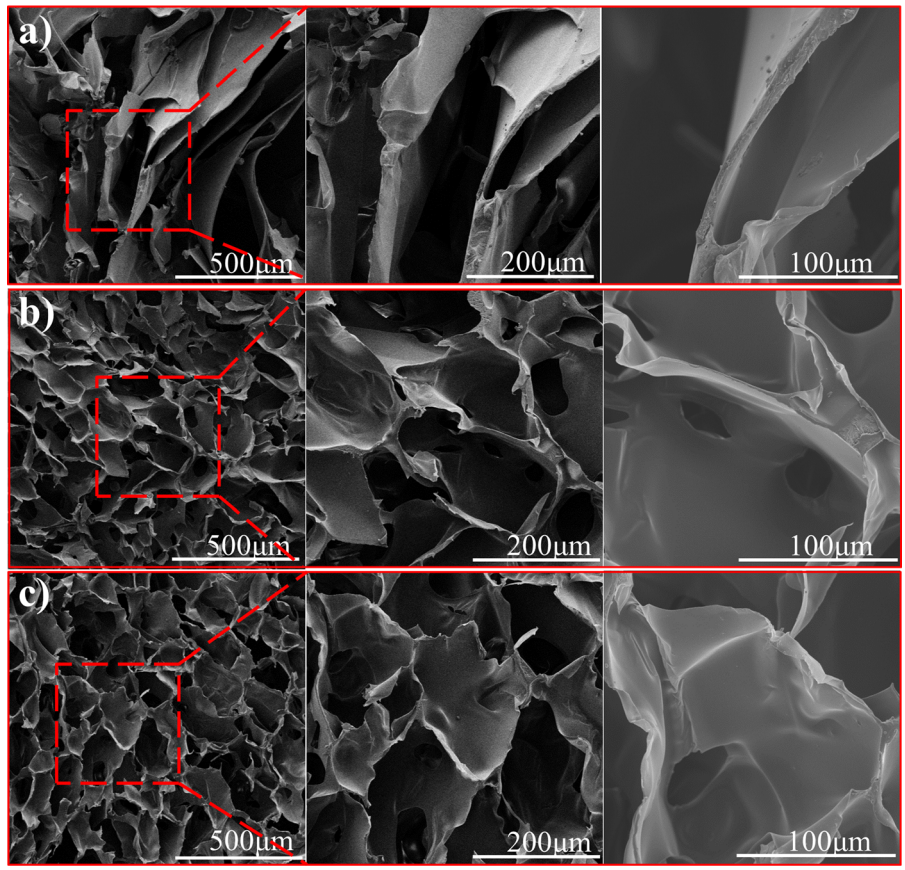

Fig. 4 SEM morphologies of the aerogels at different magnification. **a** MC/PIA-1; **b** MC/PIA-3; **c** MC/PIA-6

water mixture. Therefore, the aerogels could be a potential class of materials for oil/water separation, which have three advantages: (1) the low cost of equipment/raw materials, and facile fabrication process, (2) the simple separation process just as absorption and extrusion, (3) the high oil absorption capacity.

To verify the recyclability of aerogels, the oil absorption capacities and oil recovery ratios of each aerogel were obtained for the first five absorption-discharge cycles, shown in Fig. 7b, c. In general, MC/PIA-3 held the best oil absorption capacity, MC/PIA-1 and MC/PIA-2 took the second place, MC/PIA-4, MC/PIA-5 and MC/PIA-6 became weaken in turn. The oil absorption capacities of aerogels were related to their densities, that was, the smaller the density, the greater the capacity. The aerogel with lower density possessed more porous structure, and could accommodate more oil. For all of the aerogels, the oil absorption capacity decreased sharply after the first adsorption. During the first extrusion process, some of the lipophilic groups might be removed with the absorbed oil. The hydrophobicity of the internal structure of the aerogels decreased significantly, and resulting in a significant decrease of oil absorption capacity. For the absorption processes of second to fifth time, the oil absorption capacities had little change for each aerogel, which might be attributed to the little changes of microstructure and hydrophobicity. According to Fig. 7c, the oil recovery ratios were just about 82% for the first absorption-discharge cycle, this might be attributed to the residual oil in aerogels and the wastage during extrusion. With the increase of absorption-discharge times, the oil recovery ratio for each aerogel enhanced obviously. The total absorbed oil increased remarkably as the absorption-discharge time increased, but the residual oil in aerogels fluctuated slightly, indicating that the loss rate of oil decreased. Thus, the oil recovery ratio increased with the absorption-discharge time, and the ratio could increase to about 92 wt% when the separation times were up to five times.

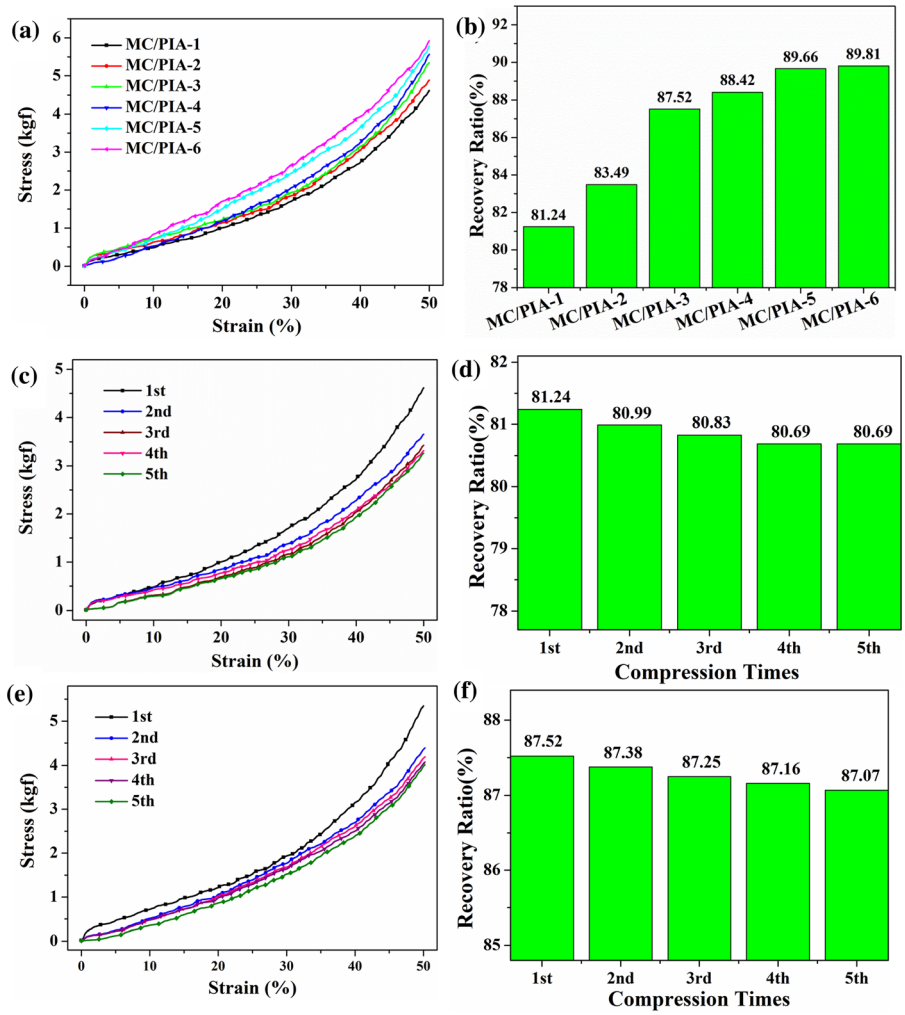

Fig. 5 The stress-strain curves (**a**) and recovery ratios (**b**) of the resulting MC/PI composite aerogels for the first compression processes. The stress-strain curves (**c**) and recovery ratios (**d**) of the resulting MC/PIA-1 with the different compression times. The stress-strain curves (**e**) and recovery ratios (**f**) of the resulting MC/PIA-3 with the different compression times

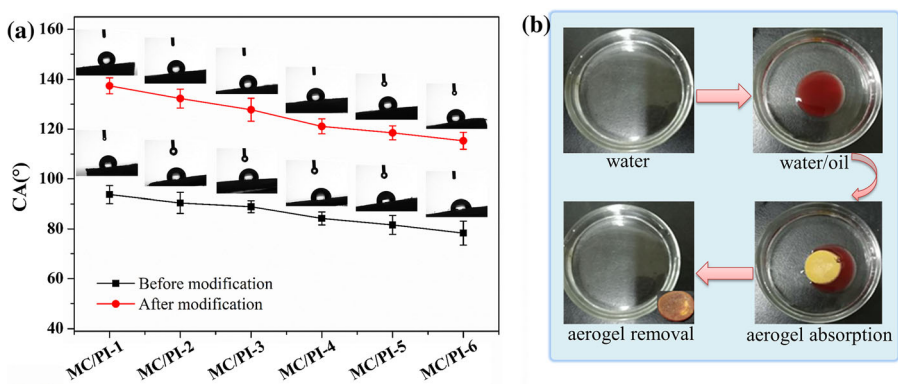

Fig. 6 **a** Water contact angles of the unmodified and modified MC/PIA-3 aerogel; **b** photographs of the removal process of methyl silicone oil (dyed with Sudan Red II) from the surface of water by the modified MC/PIA-3 aerogel

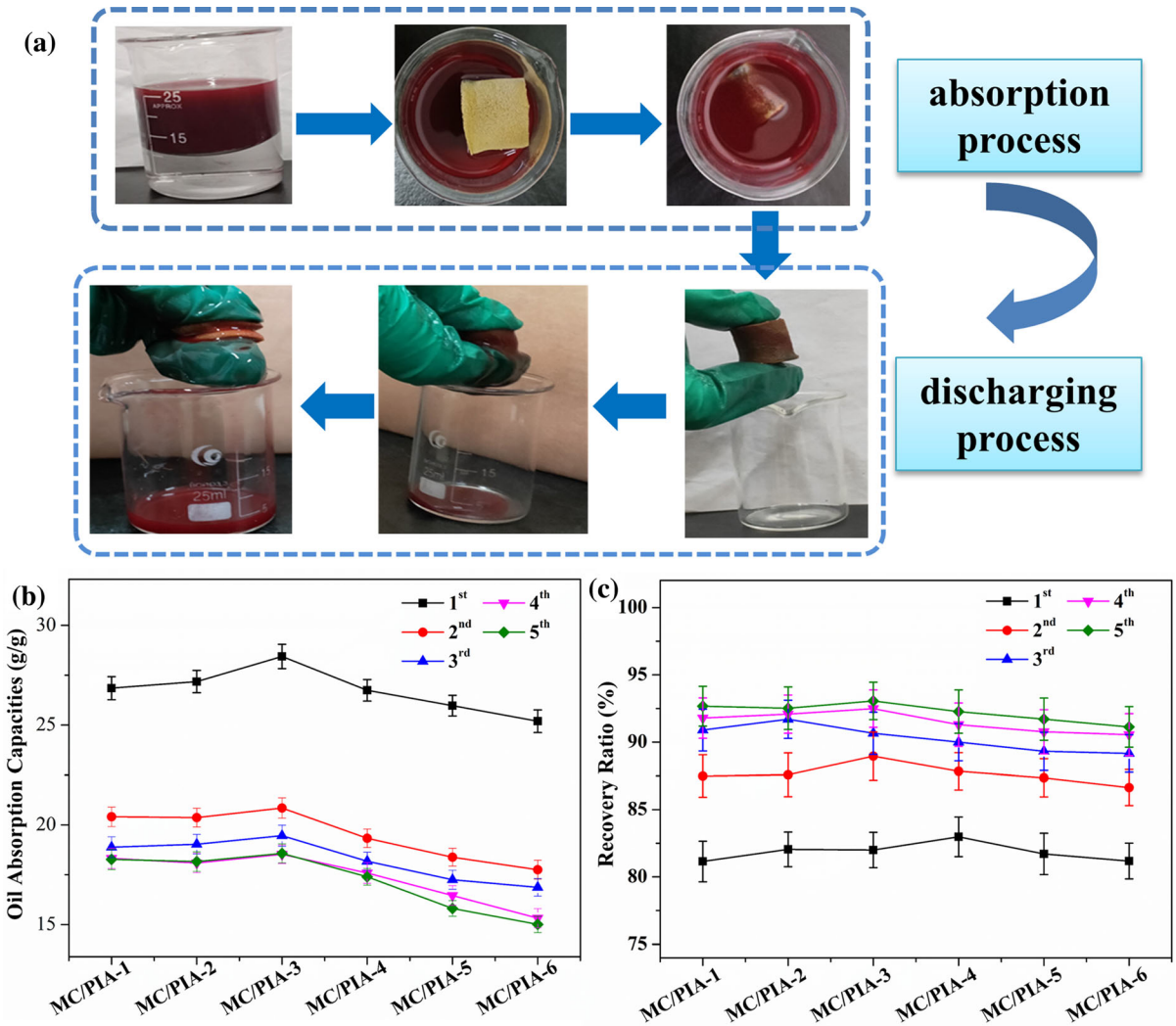

Fig. 7 **a** the absorption and discharging processes of the modified MC/PIA-3 aerogel; **b** the oil absorption capacity variations of the as-prepared aerogels for the first five absorption cycles; **c** the oil recovery ratios of the as-prepared aerogels the for the first five absorption-discharging cycles

Conclusions

In summary, a series of lightweight and porous MC/PI composite aerogels have been successfully fabricated by freeze-drying plus thermal imidization method, with subsequent TMCS functionalization. The skeleton of aerogels was effectively strengthened after incorporating with MC, and the volume shrinkage was reduced from 60.11 to 44.88%. Meanwhile, the densities decreased first and then increased in the range of 0.0309–0.0331 g/cm^3 as the MC loading increased. Otherwise, the internal defects were cured by MC, the defects of as-prepared aerogels were eliminated when the proportion of MC was beyond 10 wt%. More specifically, MC effectively strengthened the lamellar structures of the aerogels, and promoted the lateral formation of the aerogels to get reinforced concrete structure, which endowed the aerogel with robust and complete 3D porous structure, and improved the compression properties of the aerogels remarkably.

After being modified by TMCS, the functionalized aerogels exhibited much better surface hydrophobicity, as the water CA values of aerogels increased significantly by 30–40°. The low density, high porosity and surface hydrophobicity endowed the modified

aerogels excellent oil/water separation performance. The oil absorption results indicated that the modified aerogels had excellent oil absorption capacities, and the oil absorption capacity of the aerogel was mainly related to its density. For the first absorption, the oil capacities of the as-prepared aerogels were about 25.19–28.44 g/g. In addition, the oil recovery ratio increased with the absorption-discharge time, and the ratio increased by 92 wt% when the separation times were up to five times. The outstanding oil absorbency and simple process for separating oil and water with MC/PI composite aerogels are promising candidates in the field of oil/water separation.

Acknowledgments The authors are sincerely grateful for the financial support from the National Natural Science Foundation of China (Grant No. 51803110), Shaanxi Natural Science Basic Research Program (2019JQ-010, 2020JQ-724), the Opening Foundation of New Style Think Tank of Shaanxi Universities (Research Center for Auxiliary Chemistry and New Materials Development, Shaanxi University of Science and Technology, ACNM-201903), and the Opening Foundation of Key Laboratory of Auxiliary Chemistry and Technology for Chemical Industry (KFKT2019-10), the Natural Science Research Start-up Fund of Shaanxi University of Science & Technology (Grant No. 2016GBJ-06).

References

Bai Y et al (2020) Facile construction of shape-regulated beta-cyclodextrin-based supramolecular self-assemblies for drug delivery. Carbohyd Polym. https://doi.org/10.1016/j.carbpol.2019.115714

Beshkar F, Salavati-Niasari M, Amiri O (2020) Superhydrophobic-superoleophilic copper-graphite/styrene-butadiene-styrene based cotton filter for efficient separation of oil derivatives from aqueous mixtures. Cellulose 27:4691–4705. https://doi.org/10.1007/s10570-020-03112-x

Boumail A, Salmieri S, Klimas E, Tawema PO, Bouchard J, Lacroix M (2013) Characterization of trilayer antimicrobial diffusion films (ADFs) based on methylcellulose-polycaprolactone composites. J Agric Food Chem 61:811–821. https://doi.org/10.1021/jf304439s

Chao M, Li Y, Wu G, Zhou Z, Yan L (2019) Functionalized multiwalled carbon nanotube-reinforced polyimide composite films with enhanced mechanical and thermal properties. Int J Polym Sci 2019:9302803. https://doi.org/10.1155/2019/9302803

Chen X et al (2019) Highly compressible and robust polyimide/carbon nanotube composite aerogel for high-performance wearable pressure sensor. ACS Appl Mater Int 11:42594–42606. https://doi.org/10.1021/acsami.9b14688

Chhajed M, Yadav C, Agrawal AK, Maji PK (2019) Esterified superhydrophobic nanofibrillated cellulose based aerogel for oil spill treatment. Carbohyd Polym 226:115286. https://doi.org/10.1016/j.carbpol.2019.115286

Chu Z, Feng Y, Seeger S (2015) Oil/water separation with selective superantiwetting/superwetting surface materials. Angew Chem Int Edit 54:2328–2338. https://doi.org/10.1002/anie.201405785

Dashti N, Ali N, Khanafer M, Radwan SS (2019) Plant-based oil-sorbents harbor native microbial communities effective in spilled oil-bioremediation under nitrogen starvation and heavy metal-stresses. Ecotoxicol Environ Safe 181:78–88. https://doi.org/10.1016/j.ecoenv.2019.05.072

El-Shahidy MM, Shalaby ASA, Sheltawy STE (2019) Oil spills clean-up by super hydrophobic organo-modified silica aerogel monoliths treated by different solvents in ambient condition. Mater Res Express 6:105546

Gong X, Wang Y, Zeng H, Betti M, Chen L (2019) Highly porous, hydrophobic, and compressible cellulose nanocrystals/poly(vinyl alcohol) aerogels as recyclable absorbents for oil-water separation. ACS Sustain Chem Eng 7:11118–11128. https://doi.org/10.1021/acssuschemeng.9b00066

Guo X, Shan J, Lai Z, Lei W, Ding R, Zhang Y, Yang H (2018) Facile synthesis of flexible methylsilsesquioxane aerogels with surface modifications for sound-absorbance, fast dye adsorption and oil/water separation. Molecules 23:945

Gupta RK, Dunderdale GJ, England MW, Hozumi A (2017) Oil/water separation techniques: a review of recent progresses and future directions. J Mater Chem A 5:16025–16058. https://doi.org/10.1039/c7ta02070h

He X, Zhang L, Meng D, Wu J (2017) From hydrogel to aerogel: a green fabrication of multifunctional polyimide absorbents. Eur Polym J 89:461–467

Hu WJH et al (2018) An amphiphobic graphene-based hydrogel as oil-water separator and oil fence material. Chem Eng J 353:708–716. https://doi.org/10.1016/j.cej.2018.07.147

Ji L et al (2019) Enzyme cocktail containing NADH regeneration system for efficient bioremediation of oil sludge contamination. Chemosphere 233:132–139. https://doi.org/10.1016/j.chemosphere.2019.05.253

Kim TH, Jang DJ, Yang KU, Na SC, Kim DA (2009) Comparison between full-scale and model experiments of oil fences. China Ocean Eng 23:657–668

Kim J et al (2016) One-step synthesis of nano-porous monolithic polyimide aerogel. Microporous Mesoporous Mater 234:35–42. https://doi.org/10.1016/j.micromeso.2016.06.037

Krasian T, Punyodom W, Worajittiphon P (2019) A hybrid of 2D materials (MoS2 and WS2) as an effective performance enhancer for poly(lactic acid) fibrous mats in oil adsorption and oil/water separation. Chem Eng J 369:563–575. https://doi.org/10.1016/j.cej.2019.03.092

Kumar A, Negi YS, Bhardwaj NK, Choudhary V (2012) Synthesis and characterization of methylcellulose/PVA based porous composite. Carbohyd Polym 88:1364–1372. https://doi.org/10.1016/j.carbpol.2012.02.019

Kwon J, Kim J, Yoo T, Park D, Han H (2014) Preparation and characterization of spherical polyimide aerogel microparticles. Macromol Mater Eng 299:1081–1088. https://doi.org/10.1002/mame.201400010

Lin X, Hong J (2019) Recent advances in robust superwettable membranes for oil-water separation. Adv Mater

Interfaces 6:1900126. https://doi.org/10.1002/admi.201900126

Long J et al (2020) Branched sulfonated polyimide/sulfonated methylcellulose composite membranes with remarkable proton conductivity and selectivity for vanadium redox flow batteries. Chemelectrochem Early Access. https://doi.org/10.1002/celc.201901887

Machado LF, de Assis Leite DC, Coelho da Costa Rachid CT, Paes JE, Martins EF, Peixoto RS, Rosado AS (2019) Tracking mangrove oil bioremediation approaches and bacterial diversity at different depths in an in situ mesocosms system. Front Microbiol 10:2107. https://doi.org/10.3389/fmicb.2019.02107

Marrakchi F, Bouaziz M, Hameed BH (2017) Activated carbon-clay composite as an effective adsorbent from the spent bleaching sorbent of olive pomace oil: process optimization and adsorption of acid blue 29 and methylene blue. Chem Eng Res Des 128:221–230. https://doi.org/10.1016/j.cherd.2017.10.015

Mehdizadeh P, Orooji Y, Amiri O, Salavati-Niasari M, Moayedi H (2020) Green synthesis using cherry and orange juice and characterization of $TbFeO_3$ ceramic nanostructures and their application as photocatalysts under UV light for removal of organic dyes in water. J Clean Prod 252:119765. https://doi.org/10.1016/j.jclepro.2019.119765

Najafian H, Manteghi F, Beshkar F, Salavati-Niasari M (2018) Efficient degradation of azo dye pollutants on $ZnBi_{38}O_{58}$ nanostructures under visible-light irradiation. Sep Purif Technol 195:30–36. https://doi.org/10.1016/j.seppur.2017.11.076

Najafian H, Manteghi F, Beshkar F, Salavati-Niasari M (2019) Fabrication of nanocomposite photocatalyst $CuBi_2O_4/Bi_3ClO_4$ for removal of acid brown 14 as water pollutant under visible light irradiation. J Hazard Mater 361:210–220. https://doi.org/10.1016/j.jhazmat.2018.08.092

Ning T, Yang G, Wei Z, Liu X (2017) One-pot solvothermal synthesis of robust ambient-dried polyimide aerogels with morphology-enhanced superhydrophobicity for highly efficient continuous oil/water separation. React Funct Polym 116:17–23

Orooji Y, Ghasali E, Moradi M, Derakhshandeh MR, Alizadeh M, Asl MS, Ebadzadeh T (2019) Preparation of mullite-TiB_2-CNTs hybrid composite through spark plasma sintering. Ceram Int 45:16288–16296. https://doi.org/10.1016/j.ceramint.2019.05.154

Orooji Y, Ghanbari M, Amiri O, Salavati-Niasari M (2020a) Facile fabrication of silver iodide/graphitic carbon nitride nanocomposites by notable photo-catalytic performance through sunlight and antimicrobial activity. J Hazard Mater 389:122079. https://doi.org/10.1016/j.jhazmat.2020.122079

Orooji Y, Mohassel R, Amiri O, Sobhani A, Salavati-Niasari M (2020b) Gd_2ZnMnO_6/ZnO nanocomposites: green sol-gel auto-combustion synthesis, characterization and photocatalytic degradation of different dye pollutants in water. J Alloys Compd 835:155240. https://doi.org/10.1016/j.jallcom.2020.155240

Parmar KR, Dora DTK, Pant KK, Roy S (2019) An ultra-light flexible aerogel-based on methane derived CNTs as a reinforcing agent in silica-CMC matrix for efficient oil adsorption. J Hazard Mater 375:206–215. https://doi.org/10.1016/j.jhazmat.2019.04.017

Pinotti A, Garcia MA, Martino MN, Zaritzky NE (2007) Study on microstructure and physical properties of composite films based on chitosan and methylcellulose. Food Hydrocolloids 21:66–72. https://doi.org/10.1016/j.foodhyd.2006.02.001

Ranjeh M, Beshkar F, Salavati-Niasari M (2019) Sol-gel synthesis of novel Li-based boron oxides nanocomposite for photodegradation of azo-dye pollutant under UV light irradiation. Compos B Eng 172:33–40. https://doi.org/10.1016/j.compositesb.2019.05.085

Ranjeh M, Beshkar F, Amiri O, Salavati-Niasari M, Moayedi H (2020) Pechini sol-gel synthesis of Cu_2O/Li_3BO_3 and CuO/Li_3BO_3 nanocomposites for visible light-driven photocatalytic degradation of dye pollutant. J Alloys Compd 815:152451. https://doi.org/10.1016/j.jallcom.2019.152451

Ren RP, Wang Z, Ren J, Lv YK (2018) Highly compressible polyimide/graphene aerogel for efficient oil/water separation. J Mater Sci 54:5918–5926

Ren R-P, Wang Z, Ren J, Lv Y-K (2019) Highly compressible polyimide/graphene aerogel for efficient oil/water separation. J Mater Sci 54:5918–5926. https://doi.org/10.1007/s10853-018-03238-1

Seifi H, Gholami T, Seifi S, Ghoreishi SM, Salavati-Niasari M (2020) A review on current trends in thermal analysis and hyphenated techniques in the investigation of physical, mechanical and chemical properties of nanomaterials. J Anal Appl Pyrol 149:104840. https://doi.org/10.1016/j.jaap.2020.104840

Shahed GV, Taherian Z, Khataee A, Meshkani F, Orooji Y (2020) Samarium-impregnated nickel catalysts over SBA-15 in steam reforming of CH_4 process. J Ind Eng Chem 86:73–80. https://doi.org/10.1016/j.jiec.2020.02.012

Shen D, Liu J, Yang H, Yang S (2013) Intrinsically highly hydrophobic semi-alicyclic fluorinated polyimide aerogel with ultralow dielectric constants. Chem Lett 42:1230–1232

Songsaeng S, Thamyongkit P, Poompradub S (2019) Natural rubber/reduced-graphene oxide composite materials: morphological and oil adsorption properties for treatment of oil spills. J Adv Res 20:79–89. https://doi.org/10.1016/j.jare.2019.05.007

Sun J, Xu Y, Chen H, Tan Z, Fan L (2014) Synthesis and properties of high oil-absorbing resins with long chain by high internal phase emulsions as template. Sep Sci Technol 49:2518–2524. https://doi.org/10.1080/01496395.2014.928322

Wang W, Zheng Y, Lee K (2013) Chemical dispersion of oil with mineral fines in a low temperature environment. Mar Pollut Bull 72:205–212. https://doi.org/10.1016/j.marpolbul.2013.03.042

Wang Y, Ge Q, Chen X, Qi S, Tian G, Wu D (2017) Ultralight and flexible MWNTs/polyimide hybrid aerogels for elastic conductors. Macromol Mater Eng. https://doi.org/10.1002/mame.201700082

Wang D-C, Yang X, Yu H-Y, Gu J, Qi D, Yao J, Ni Q (2020a) Smart nonwoven fabric with reversibly dual-stimuli responsive wettability for intelligent oil-water separation

and pollutants removal. J Hazard Mater 383:121123. https://doi.org/10.1016/j.jhazmat.2019.121123

Wang F, Luo S, Xiao S, Zhang W, Zhuo Y, He J, Zhang Z (2020b) Enabling phase transition of infused lubricant in porous structure for exceptional oil/water separation. J Hazard Mater 390:122176. https://doi.org/10.1016/j.jhazmat.2020.122176

Wang Y, Cui Y, Shao Z, Gao W, Fan W, Liu T, Bai H (2020) Multifunctional polyimide aerogel textile inspired by polar bear hair for thermoregulation in extreme environments. Chem Eng J. https://doi.org/10.1016/j.cej.2020.124623

Xu X et al (2019) Preparation and characterization of cellulose grafted with epoxidized soybean oil aerogels for oil-absorbing materials. J Agric Food Chem 67:637–643

Yan D, Meng L, Li H, Song T, Su P, Bao M, Li X (2019a) Petroleum hydrocarbon release behavior study in oil-sediment aggregates: turbulence intensity and chemical dispersion effect. RSC Adv 9:7922–7931. https://doi.org/10.1039/c8ra08871c

Yan L et al (2019b) Robust construction of underwater superoleophobic CNTs/nanoparticles multifunctional hybrid membranes via interception effect for oily wastewater purification. J Membr Sci 569:32–40

Yang WJ et al (2019) Recent progress in bio-based aerogel absorbents for oil/water separation. Cellulose 26:6449–6476

Yuan C, Emelianov DA, Varfolomeev MA, Abaas M (2019) Combustion behavior of aromatics and their interaction with n-alkane in in-situ combustion enhanced oil recovery process: thermochemistry. J Ind Eng Chem 76:467–475. https://doi.org/10.1016/j.jiec.2019.04.014

Yuan S, Jiang H, Shi Y, Ren Z, Wang J, Zhang Y (2019b) Study on heavy oil components transformation path based on core analysis during in-situ combustion process. Fuel 253:72–78. https://doi.org/10.1016/j.fuel.2019.04.135

Zhai C, Jana SC (2017) Tuning porous networks in polyimide aerogels for airborne nanoparticle filtration. ACS Appl Mater Int 9:30074–30082. https://doi.org/10.1021/acsami.7b09345

Zhang X, Liu J, Yang S (2016) Synthesis and characterization of flexible and high-temperature resistant polyimide aerogel with ultra-low dielectric constant. Express Polym Lett 10:789–798

Zhang Y, Yin M, Lin X, Ren X, Huang T-S, Kim IS (2019) Functional nanocomposite aerogels based on nanocrystalline cellulose for selective oil/water separation and antibacterial applications. Chem Eng J 371:306–313. https://doi.org/10.1016/j.cej.2019.04.075

Zhang X, Li W, Song P, You B, Sun G (2020) Double-cross-linking strategy for preparing flexible, robust, and multifunctional polyimide aerogel. Chem Eng J. https://doi.org/10.1016/j.cej.2019.122784

Zhao L, Zheng Q, Liu Y, Wang S, Wang J, Liu X (2020) Enhanced strength and toughness of κ-carrageenan/polyacrylic acid physical double-network hydrogels by dual cross-linking of the first network. Eur Polym J 124:109474. https://doi.org/10.1021/acs.macromol.8b02269

Zhao Y et al (2019) Amphiphilic graphene aerogel with high oil and water adsorption capacity and high contact area for interface reaction. ACS Appl Mater Int 11:22794–22800